Interfacial thermal conductance across metal-insulator/semiconductor interfaces due to surface states

Tingyu Lu,[1] Jun Zhou,[1,*] Tsuneyoshi Nakayama,[1,2] Ronggui Yang,[3,4] and Baowen Li[3]

[1]*Center for Phononics and Thermal Energy Science, School of Physics Science and Engineering, Tongji University, Shanghai 200092, People's Republic of China*
[2]*Hokkaido University, Sapporo 060-0826, Japan*
[3]*Department of Mechanical Engineering, University of Colorado, Boulder, Colorado 80309, USA*
[4]*Materials Science and Engineering Program, University of Colorado, Boulder, Colorado 80309, USA*

We point out that the effective channel for the interfacial thermal conductance, the inverse of Kapitza resistance, of metal-insulator/semiconductor interfaces is governed by the electron-phonon interaction mediated by the surface states allowed in a thin region near the interface. Our detailed calculations demonstrate that the interfacial thermal conductance across Pb/Pt/Al/Au-diamond interfaces are only slightly different among these metals, and reproduce well the experimental results of the interfacial thermal conductance across metal-diamond interfaces observed by Stoner *et al.* [Phys. Rev. Lett. **68**, 1563 (1992)] and most recently by Hohensee *et al.* [Nat. Commun. **6**, 6578 (2015)].

I. INTRODUCTION

Kapitza resistance, which occurs when heat flows across two different materials, was first observed by the measurement of the temperature jump at solid-liquid helium interfaces [1,2]. Interfacial thermal conductance (ITC), the inverse of Kapitza resistance, between solid-solid interfaces has been the most intensive research topic in the thermal transport community over the past two decades for thermal management of nanoelectronics and for engineering nanostructured materials for thermoelectrics and for superior thermal insulators [3–7]. Overheating caused by heat accumulation due to the presence of Kapitza resistance is a major obstacle to improving the performance and the reliability of nanoelectronic and optoelectronic devices. It is of great importance to understand the underlying mechanisms of Kapitza resistance or ITC across solid-solid interfaces.

Compared to nonmetal interfaces, the heat conduction mechanism across metal-insulator/semiconductor interfaces is much more complicated since it involves energy conversion and coupling among different energy carriers where electrons are the major heat carriers in metals and phonons are the major heat carriers in the insulator/semiconductor. The applicability of various proposed mechanisms has been debated for decades [5].

Swartz and Pohl [5] proposed diffusive phonon scattering at interfaces as an extension of the acoustic mismatch theory for solid-liquid interfaces proposed by Khalatonikov [8], which takes into account the elastic scattering of phonons by the roughness of interfaces. However, the predicted ITC values based on this theory are quite different from the measured values at room temperature. Stoner *et al.* [9] measured ITC across a large series of metal (Pb/Ti/Al/Au)-insulator (diamond/sapphire/BaF$_2$) interfaces using a picosecond laser-based pump-and-probe technique. They found that ITC across

the Pb-diamond interface was significantly larger than the radiation limit of phonon transmission, which considers the maximum possibility of phonon transmission. To overcome the underestimation of ITC, multiphonon scattering due to anharmonicity was then proposed, which provides an additional energy transfer channel across an interface. However, one would expect ITC to be reduced in the presence of pressure if anharmonicity is important, as the anharmonicity of diamond would be suppressed by pressure [10]. This prediction contradicts with a recent experimental exploration where pressure-dependent ITC across a metal-diamond interface was measured by Hohensee *et al.* [11].

On the other hand, due to the existence of electrons in the metal side, the role of the electron-phonon (*e*-*p*) interaction between the electrons in metals and phonons in nonmetals has been considered, which was first introduced for metal-helium interfaces and then extended to metal-insulator/semiconductor interfaces. The theoretical framework of the *e*-*p* interaction of the metal-helium interface was proposed by Little [12] and Andreev [13] in the 1960s and experimentally proved by Wagner *et al.* [14] through the observation of ITC dependence on the applied magnetic field.

Energy coupling between electrons and phonons in bulk materials was modeled by Kaganov [15] and Allen [16] several decades ago. For the *e*-*p* interaction of metal-insulator/semiconductor interfaces, there are several different models which show different mechanisms of interactions. In the 1990s, Huberman and Overhauser [17] calculated the ITC across a Pb-diamond interface by taking into account the coupling between the free electrons in Pb and joint vibrational modes near the interface. In their work, they assumed that the phonon modes of an insulator can extend into the metal side with an attenuation rate. Sergeev [18] has proposed a model to incorporate the inelastic electron-boundary scattering in a similar way as the inelastic electron-impurity scattering. This model usually overestimates the ITC since all the atoms on the insulator/semiconductor side are treated as impurities. Mahan [19] has proposed a mechanism for the *e*-*p* interaction by introducing image charges, which is likely inapplicable

---

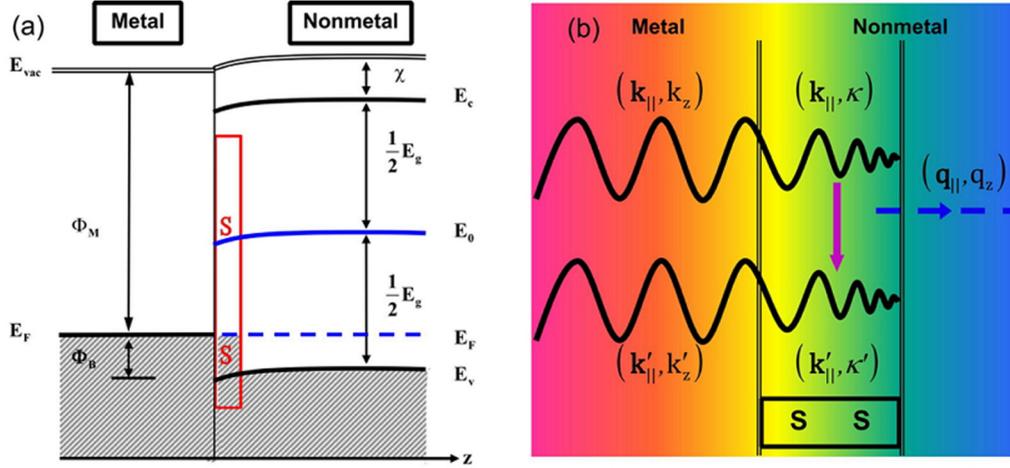*Author to whom correspondence should be addressed: zhoujunzhou@tongji.edu.cn

085433-1

FIG. 1. (a) Band alignment of a metal-diamond interface along the z direction. The SS only exists in a thin interfacial region, as shown. (b) Schematic of phonon emission due to the SS-phonon interaction. $(\mathbf{q}_\|,q_z)$ denotes the wave vector of the phonon, where $\mathbf{q}_\|$ is in the $x-y$ plane and q_z is in the z direction. $(\mathbf{k}_\|,\kappa)$ and $(\mathbf{k}_\|',\kappa')$ are the wave vectors of the initial and final electron states of SS, respectively. $(\mathbf{k}_\|,k_z)$ and $(\mathbf{k}_\|',k'_z)$ are the related wave vectors of electrons in metal.

to nonpolar materials, such as diamond. Giri *et al.* [20] considered the electronic transmission probability, which is a fitting parameter, to calculate ITC. One important observation is that most of the above theories, except Mahan's, predict a very strong dependence of ITC on the electronic structure, which is in contradiction with experimental results [9,11,21]. For example, the calculated ITC across the Pb-diamond interface is two orders of magnitude larger than that across a Bi-diamond interface, whereas very similar measured values have been obtained [21]. Most recently, Hohensee *et al.* [11] have measured the ITC across interfaces between various metals (Pb/Pt/Al/Au) and diamond at high pressures of up to 50 GPa. They found that ITC converges to similar values at high pressures among Pb/Pt/Al/Au.

The discrepancy between theoretical prediction and experimental observation of ITC across a metal-insulator/ semiconductor interface due to an e-p interaction between the electrons in metals and phonons in an insulator/semiconductor is still an outstanding question. Most theories assumed that free electrons from the metal side are incident on the interface and are then reflected back while interacting with phonons at an interface [17,18,20]. This assumption could be wrong in realistic materials.

In this paper, we propose a mechanism that determines the e-p interaction across metal-insulator/semiconductor interfaces near room temperature, which is mediated by the surface states (SS) [22]. The SS are localized electron states in the insulator/semiconductor induced by electrons from the metal side, whose wave functions decay exponentially from the interface [23,24] with a decay length of around several angstroms. This heat conduction channel, due to the interaction of SS electrons with phonons in the insulator/semiconductor side, which is denoted as a SS-phonon interaction in this paper, should be considered in parallel with phonon transmission-mediated thermal conductance [25,26]. When this channel dominates, we find that ITC across Pb/Pt/Al/Au-diamond interfaces varies only slightly among different metals with a large difference in electronic structures, which agree well with the experimental

results [9,11,21]. This theory also gives a sound explanation for the recently measured ITC under high pressures [11].

This paper is organized as follows. We present the model to calculate ITC due to the SS-phonon interaction in Sec. II. This model is then used to calculate the ITC across Pb/Pt/Al/Au-diamond interfaces in comparison with experimental data from the literature in Sec. III. Finally, Sec. IV concludes this paper.

II. MODEL

The SS exist in a very thin region near the interface that should play a crucial role in the energy exchange between the electrons in the metals and phonons in the insulator/semiconductor. To simplify the modeling, we chose diamond as an example in this study. Our model can be easily extended to other materials when SS are important.

Figure 1(a) shows the band alignment of a metal-diamond interface where E_F is the Fermi energy, Φ_M is the work function of metal, E_g is the band gap with E_0 as its center, χ is the electron affinity, Φ_B is the Schottky barrier height, E_{vac} is the vacuum energy level, and E_c and E_v are the conduction and valence band edges, respectively. The band bending near the surface originates from the charge transfer between the metal and diamond where a p-type diamond with boron doping is chosen as an example. E_F is usually pinned at the surface to the SS [27].

The temperature of the electrons in SS could be different from the temperature of electrons near the surface in the metal due to the existence of interfacial electronic thermal resistance. In order to simplify the investigation, we neglect here the difference between these two temperatures since the electronic thermal resistance is believed to be smaller than the resistance due to the SS-phonon interaction. The net heat flux from SS electrons to phonons in the insulator/semiconductor due to the SS-phonon interaction is given by $\Delta \dot{Q}_{NM}$, where T_e and T_p are the electron and phonon temperatures, respectively [2,17]. Then the ITC (h_K) due to the SS-phonon interaction is defined
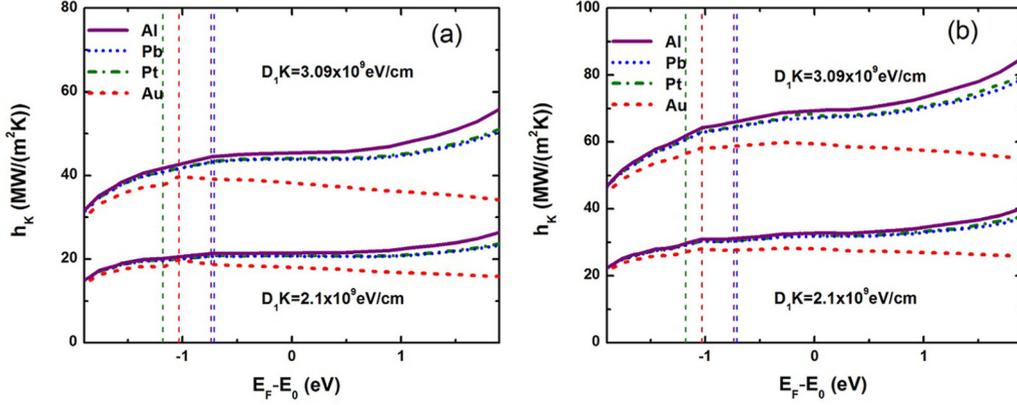
FIG. 2. Calculated ITC across Pb/Pt/Al/Au-diamond interfaces for (a) free phonon modes and (b) localized phonon modes as a function of $E_F - E_0$ for two different values of $D_1 K$ when $T_p = 293$ K. The realistic $E_F - E_0$ listed in Table I are marked with vertical lines and the corresponding ITC are shown in Table II.

by

$$h_K = \Delta \dot{Q}_{NM} / \Delta T, \quad \Delta T = T_e - T_p \ll T_e, T_p. \quad (1)$$

$\Delta \dot{Q}_{NM}$ defined in Eq. (1) can be calculated by [19,28]

$$\Delta \dot{Q}_{NM} = \frac{2\pi}{\hbar} \sum_{\lambda, \mathbf{k}_\parallel, \kappa, \kappa', \mathbf{q}_\parallel, q_z} \hbar \omega_{\lambda, q_\parallel, q_z} |M_\lambda(q_\parallel, q_z)|^2$$

$$\times |I(k'_\parallel, k_\parallel, \kappa', \kappa, q_z)|^2 W, \quad (2)$$

where $\hbar$ is the Planck constant, $\hbar \omega_{\lambda, q_\parallel, q_z}$ is the phonon energy with polarization index λ in the insulator/semiconductor, $M_\lambda(q_\parallel, q_z)$ are the scattering matrix elements, and $I(k'_\parallel, k_\parallel, \kappa', \kappa, q_z)$ is the form factor. The transition probability W is given by

$$W = \delta\big(\varepsilon_{k_\parallel, \kappa} - \varepsilon_{\mathbf{k}_\parallel + \mathbf{q}_\parallel, \kappa'} - \hbar\omega_{\lambda, q_\parallel, q_z}\big)\big[f_{k_\parallel, k_z}(1 - f_{\mathbf{k}_\parallel + \mathbf{q}_\parallel, \kappa'})$$

$$\times \big(n_{\lambda, q_\parallel, q_z} + 1\big) - f_{\mathbf{k}_\parallel + \mathbf{q}_\parallel, \kappa'}\big(1 - f_{k_\parallel, k_z}\big)n_{\lambda, q_\parallel, q_z}\big]$$

$$- \delta\big(\varepsilon_{k_\parallel, k_z} - \varepsilon_{\mathbf{k}_\parallel + \mathbf{q}_\parallel, \kappa'} + \hbar\omega_{\lambda, q_\parallel, q_z}\big)\big[f_{k_\parallel, k_z}(1 - f_{\mathbf{k}_\parallel + \mathbf{q}_\parallel, \kappa'})$$

$$\times n_{\lambda, q_\parallel, q_z} - f_{\mathbf{k}_\parallel + \mathbf{q}_\parallel, \kappa'}\big(1 - f_{k_\parallel, k_z}\big)\big(n_{\lambda, q_\parallel, q_z} + 1\big)\big]. \quad (3)$$

Here, $f_{k_\parallel, \kappa}(T_e) = \{\exp[(\varepsilon_{k_\parallel, \kappa} - E_F)/(k_B T_e)] + 1\}^{-1}$ is the Fermi-Dirac distribution function, where $\varepsilon_{k_\parallel, \kappa}$ is the electron energy and k_B is the Boltzmann constant, and $n_{\lambda, q_\parallel, q_z}(T_p) = \{\exp[(\hbar\omega_{\lambda, q_\parallel, q_z})/(k_B T_p)] - 1\}^{-1}$ is the Bose-Einstein distribution function.

The second quantized form of the SS-phonon interaction Hamiltonian is written as

$$H = \sum_{\lambda, \mathbf{k}_\parallel, \kappa, \kappa', \mathbf{q}_\parallel, q_z} M_\lambda(q_\parallel, q_z) I(k'_\parallel, k_\parallel, \kappa', \kappa, q_z) c^\dagger_{\mathbf{k}_\parallel + \mathbf{q}_\parallel, \kappa'} c_{\mathbf{k}_\parallel, \kappa}$$

$$\times \big[a_{\lambda, \mathbf{q}_\parallel, q_z} + a^\dagger_{\lambda, -\mathbf{q}_\parallel, -q_z}\big], \quad (4)$$

where $c^\dagger$ ($a^\dagger$) and c (a) are the creation and annihilation operators of electrons (phonons), respectively. In Fig. 1(b), we show the phonon emission process when the electron is scattered from state $(\mathbf{k}_\parallel, \kappa)$ to state $(\mathbf{k}'_\parallel, \kappa')$. We consider the phonon modes in the insulator/semiconductor side because SS mainly exist in a thin region in the insulator/semiconductor.

Several methods have been proposed to calculate SS, such as electron wave function matching, Green's function

matching [24], and the self-consistent pseudopotential method [22]. We use the simplest one-dimensional electron wave function matching method by considering a periodic potential $V_0 \cos(gz)(V_0 < 0)$ along the z direction when electrons are assumed to be free in the x-y plane [24]. $g = 2\pi/(a/2)$ is the reciprocal lattice vector of diamond along the (001) direction with a lattice constant $b = a/2$. Then the electron wave function in the band gap of the insulator/semiconductor is $\psi_{\mathbf{k}_\parallel, \kappa}(\mathbf{r}) = S^{-1/2} B e^{i\mathbf{k}_\parallel \cdot \boldsymbol{\rho}} \varphi(\kappa, z)$ for $z \geqslant 0$, where S is the area of the interface and B is a normalization factor. $\varphi(\kappa, z) = e^{-\kappa z} \cos(gz/2 + \phi/2)$, where ϕ is a phase shift. The positional coordinate is $\mathbf{r} = (\boldsymbol{\rho}, z)$. For a given κ, there are two energy states, $\varepsilon_{k_\parallel, \kappa} \approx E_0 + \frac{\hbar^2 k_\parallel^2}{2m} \pm |\xi|$, where E_0 is the center of the gap and $|\xi| = \sqrt{V_0^2 - \frac{\hbar^4 \kappa^2 g^2}{2m}}$. We focus our study on the localized SS electrons which require $-|V_0| < \xi < |V_0|$. The electron wave function in the metal is written as $\psi^M_{\mathbf{k}_\parallel, \kappa}(\mathbf{r}) = S^{-1/2} A e^{i\mathbf{k}_\parallel \cdot \boldsymbol{\rho}} \sin(k_z z + \eta)$ for $z \leqslant 0$, where A is the normalization factor, and η is a phase shift. For a given k_F, we have $k_z = \sqrt{k_F^2 - k_\parallel^2}$ and $k'_z = \sqrt{k_F^2 - |\mathbf{k}_\parallel + \mathbf{q}_\parallel|^2}$.

The form factor for free phonon modes is then written as $I(k'_\parallel, k_\parallel, \kappa', \kappa, q_z) = B B'^* \int_0^\infty dz \varphi^*(\kappa', z) e^{iq_z z} \varphi(\kappa, z)$. Here, only the electrons at the insulator/semiconductor side ($z > 0$) contribute to the ITC and the contribution from the metal side is negligible. The reason is that the e-p interaction for $z < 0$ is merely the conventional e-p interaction in the metal which does not directly contribute to ITC [29]. One can easily modify $e^{iq_z z}$ in the phonon wave function to $\sin(q_z z)$ to consider the localized phonon modes [19]. The detailed expressions of the form factors for both cases are shown in the Appendix.

TABLE I. Fermi wave vectors, Schottky barrier heights, and corresponding $E_F - E_0$ used in the calculations.

Parameters	Pb	Pt	Al	Au
$k_F(\text{Å}^{-1})$	1.58 [33]	1.6 [34]	1.75 [33]	1.21 [33]
Φ_B (eV)	2.03 [35]	1.56 [35]	2.0 [35]	1.71 [35]
$E_F - E_0$ (eV)	−0.71	−1.18	−0.74	−1.03

TABLE II. Calculated ITC across Pb/Pt/Al/Au-diamond interfaces at room temperature for free and localized phonon modes when $D_1K = 3.09 \times 10^9$ eV/cm. ITC from DMM and phonon radiation limit, and experimental measured values are listed for comparison. The unit is [MW/(m² K)].

ITC	Pb	Au	Pt	Al
SS-free phonon	43.3	39.7	41	44.4
SS-localized phonon	64.5	58.3	61.2	65.9
DMM	2 [9]	12 [9]	35 [26]	130 [26]
Radiation limits	2.5 [9]	24 [9]	47 [11]	207 [11]
Experimental data	31 [9], 60 [11]	40 [9], 62 [11]	143 [11]	46 [9], 153 [11], 23–180 [38]

III. RESULTS AND DISCUSSIONS

We now turn to the calculation of ITC due to the interaction of SS electrons with phonons across metal-diamond interfaces. We choose $|V_0| = E_g/2 = 2.74$ eV for diamond [30]. We calculate the SS-phonon interaction due to both acoustic and optical modes by employing the deformation potentials. For longitudinal-acoustic (LA) modes, the squared scattering matrix elements are $|M_{LA}(q_{||}, q_z)|^2 = \hbar D^2 q/(2V\rho_0 v_l)$ [31], where D is the deformation potential constant of the acoustic phonons, ρ_0 is the mass density, v_l is the longitudinal sound velocity, and V is the volume. The transverse-acoustic phonon modes are considered similarly by using the transverse sound velocity v_t. The optical-phonon scattering with a polar interaction is irrelevant since diamond is a nonpolar material. The squared scattering matrix elements of electron-longitudinal optical (OP) phonon scattering with a deformation potential are $|M_{OP}(q_{||}, q_z)|^2 = \hbar(D_1K)^2/(2V\rho_0\omega_{OP})$ [30], where D_1K is the optical deformation potential constant, and ω_{OP} is the optical phonon frequency. The contributions from the two transverse optical phonon modes are considered similarly. These parameters of diamond are used: $a = 3.567$ Å, $v_l = 1.82 \times 10^4$ m/s, $v_t = 1.23 \times 10^4$ m/s, $\rho_0 = 3.515$ g/cm³, and $D = 8.7$ eV [32].

Figure 2 shows the calculated ITC across Pb/Pt/Al/Au-diamond interfaces as a function of $E_F - E_0$ when $T_p = 273$ K. ITC considering both free and localized phonon modes are shown in Figs. 2(a) and 2(b), respectively. Two different optical deformation potentials are considered. One is $D_1K = 2.1 \times 10^9$ eV/cm, which comes from transport property mea-

surements [36], and the other is $D_1K = 3.09 \times 10^9$ eV/cm, which comes from Raman experiments [37]. The Fermi wave vectors of metals used in the calculation are shown in Table I. We find that ITC for all four interfaces varies with $E_F - E_0$ because the SS and the form factor are energy dependent, which will be shown later.

For most metal-insulator/semiconductor interfaces, E_F is pinned at the surface to the SS in the band gap [23]. Such a pinning effect is characterized by the Schottky barrier height which enables us to approximately deduce the realistic $E_F - E_0$ by $\Phi_B - E_g/2$, as shown in Fig. 1(a). The Φ_B values of the four interfaces and the corresponding $E_F - E_0$ are listed in Table I. We mark these $E_F - E_0$ values with vertical lines in Figs. 2(a) and 2(b). With the obtained $E_F - E_0$, we find that ITC for Pb/Pt/Al/Au-diamond interfaces varies from 39.7 to 44.4 MW/(m² K) for free phonon modes and from 58.3 to 65.9 MW/(m² K) for localized phonon modes, as shown in Table II. The ITC with localized phonon modes is about 50% larger than that with free phonon modes. For both cases, the differences between the different metals are found to be slight because of the similar Fermi wave vectors and Fermi energies in the gap. This finding explains well why the ITC approaches similar values at high pressures [11].

We further compare ITC due to SS-phonon interactions with a parallel channel of phonon transmission-induced ITC which is calculated by the diffuse mismatch model (DMM) and by the phonon radiation limit in Table II. The experimental data are also shown. For Pb/Au-diamond interfaces, our calculated ITC is much larger than that from DMM and is in good agreement
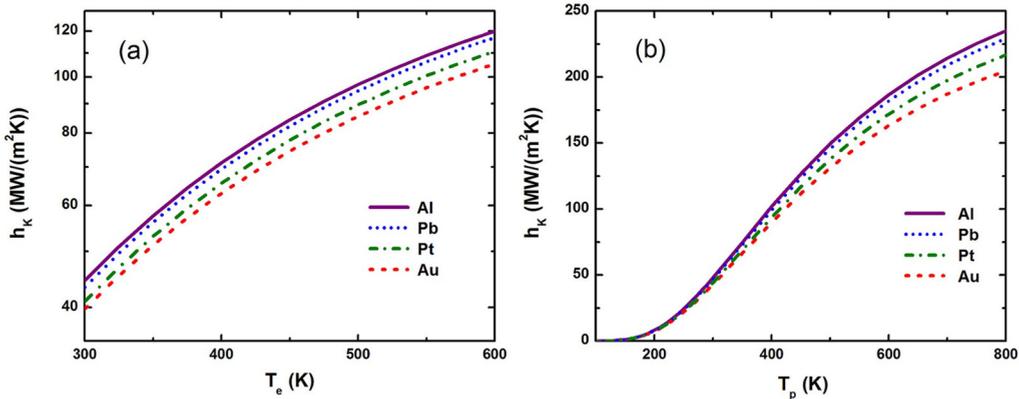

FIG. 3. Temperature dependence of ITC across Pb/Pt/Al/Au-diamond interfaces with $D_1K = 3.09 \times 10^9$ eV/cm. (a) When $T_p = 293$ K, h_K increases with T_e because of more participating electron states at higher temperatures. (b) h_K dependence on T_p for small ΔT. The increased phonon population at higher T_p leads to more energy transfer.
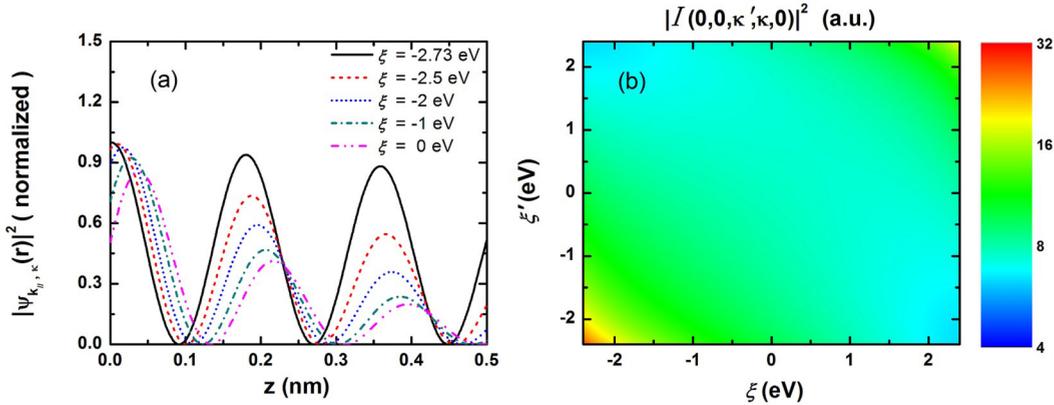
FIG. 4. (a) Spatial variations of normalized modular square of the SS for different energy ξ. $|\psi_{\mathbf{k}_{||},\kappa}(\mathbf{r})|^2$ decays more significantly when the energy is at the middle of the band gap than that with the energy near the band edge. (b) Modular square of form factor $|I(0,0,\kappa',\kappa,0)|^2$ as a function of ξ and ξ'. Changes in $|I(0,0,\kappa',\kappa,0)|^2$ are significant when $|\xi'| \sim |V_0|$ and $|\xi| \sim |V_0|$ while they are slight when $|\xi'| \ll |V_0|$ and $|\xi| \ll |V_0|$.

with experimental data. This comparison indicates that a SS-phonon interaction dominates the ITC of these two interfaces and the contribution from phonon transmission is negligible. For Pt-diamond interfaces, our calculated ITC is comparable to that from DMM and the phonon radiation limit and they must be considered in parallel. The summation of the ITC from the two channels varies from 76 to 96.2 MW/(m² K), which is 50%–65% of the experimental data. For the Al-diamond interface, our calculated ITC is 30%–50% of that from DMM. The summation of the ITC from the two channels varies from 174.4 to 195.9 MW/(m² K), which is close to the measured data from Ref. [11] and the maximum value in Ref. [38]. This finding implies that both the SS-phonon interaction and phonon transmission should be considered in parallel [25,26] for Pt/Al-diamond interfaces.

Figure 3 shows the temperature dependence of ITC across Pb/Pt/Al/Au-diamond interfaces when $D_1 K = 3.09 \times 10^9$ eV/cm and $E_F - E_0$ in Table I are used. Figure 3(a) shows the dependence of ITC on T_e when $T_p = 293$ K. We find that h_K increases with T_e for all metals since more SS electrons participate in the e-p interaction at higher temperatures. This is quite different from the e-p coupling constant in bulk metals, which remains almost constant at room temperature [19]. Figure 3(b) shows the dependence of h_K on T_p. We find that h_K increases with T_p for all interfaces, because the increased phonon population at higher T_p leads to a stronger e-p interaction and provides more energy transfer channels.

In order to better understand the dependence of ITC on Fermi energy and temperature, as shown in Figs. 2 and 3, we show the energy dependence of $|\psi_{\mathbf{k}_{||},\kappa}(\mathbf{r})|^2$ in Fig. 4(a) and the energy dependence of normalized $|I(k'_{||},k_{||},\kappa',\kappa,q_z)|^2$ in Fig. 4(b). Figure 4(a) shows that $|\psi_{\mathbf{k}_{||},\kappa}(\mathbf{r})|^2$ decays significantly when $\xi = 0$, where κ reaches its maximum, $2m|V_0|/(\hbar^2 g)$. When $|\xi|$ increases, the corresponding κ decreases and finally vanishes when $|\xi| = |V_0|$. Remember that $\pm|\xi|$ results in the same κ, therefore the $\xi > 0$ case has a similar trend, which is not shown in this figure. The ITC highly depends on the square of the modules of the form factor as shown in Eq. (2). Figure 4(b) shows $|I(k'_{||},k_{||},\kappa',\kappa,q_z)|^2$ as a function of the energies of initial state (ξ) and final

state (ξ') for a long phonon wavelength limit, $q_z \to 0$, when $k_z = k'_z = k_F$. We find that $|I(0,0,\kappa',\kappa,0)|^2$ in the band gap changes slightly when the energy is deep inside the band gap, $|\xi'| \ll |V_0|$ and $|\xi| \ll |V_0|$. A significant increase of the form factor only occurs when $|\xi'| \sim |V_0|$ and $|\xi| \sim |V_0|$. The metals we considered here have similar Fermi energies, which are about 1 eV below the gap center, as shown in Table I. Therefore, the form factor with a Fermi energy $\xi \sim \xi' \sim -1$ eV should dominate the ITC.

IV. SUMMARY

In summary, we have calculated the ITC across metal-insulator/semiconductor interfaces by considering the electron-phonon interaction between surface state electrons and phonons in the insulator/semiconductor. The calculated ITC across Pb/Pt/Al/Au-diamond interfaces is very close among these metals, even though the electronic structures of these metals are quite different. The main reason is the pinning of the Fermi energy in the band gap. This finding explains well the experimental results obtained by Stoner *et al.* [9] and by Hohensee *et al.* [11].

APPENDIX: EXPRESSIONS OF FORM FACTORS

For free phonon modes, the square of the modules of the form factor can be expressed as $|I(k'_{||},k_{||},\kappa',\kappa,q_z)|^2 = |B|^2|B'|^2 \Xi/16$. In the calculation, the normalization factor B should be determined by matching the electron wave functions at $z = 0$. For a semi-infinite metal, we have

$A \to \sqrt{2/L_M}$ and $|B| \to A|\sin \eta / \cos(\phi/2)|$. $|B|$ is determined by η and ϕ, which can be calculated by solving [22]

$$e^{i\phi} = \cos \phi + i \sin \phi = \left(\xi + i\sqrt{V_0^2 - \xi^2}\right)/V_0, \tag{A1a}$$

$$\tan \eta = \frac{-2k_z}{g \tan \left(\frac{\phi}{2}\right) + 2\kappa}. \tag{A1b}$$

Here, $\phi = 2n\pi + \tan^{-1}(\sqrt{V_0^2 - \xi^2}/\xi)$ for $\xi \leqslant 0$ and $\phi = (2n+1)\pi + \tan^{-1}(\sqrt{V_0^2 - \xi^2}/\xi)$ for $\xi > 0$, where n is an arbitrary integer. $|B'|$ and ϕ' can be calculated similarly by changing ξ to ξ'.

We note $\tilde{\kappa} = \kappa + \kappa'$, $\gamma_1 = q_z^2 + \tilde{\kappa}^2 - g^2$, $\gamma_2 = g\tilde{\kappa}$, $\gamma_3 = q_z^4 + \tilde{\kappa}^4 - g^2\tilde{\kappa}^2 - g^2 q_z^2 + 2q_z^2\tilde{\kappa}^2$, and $\gamma_4 = 2g\tilde{\kappa}^3 + 2gq_z^2\tilde{\kappa}$. $\Xi = \Xi_1 + \Xi_2 + \Xi_3 + \Xi_4$ can be expressed in terms of

$$\Xi_1 = \frac{1}{(q_z + g)^2 + \tilde{\kappa}^2} + \frac{1}{(q_z - g)^2 + \tilde{\kappa}^2} + \frac{2}{q_z^2 + \tilde{\kappa}^2}, \tag{A2a}$$

$$\Xi_2 = \frac{2\gamma_1 \cos(\phi + \phi') - 4\gamma_2 \sin(\phi + \phi')}{\gamma_1^2 + 4\gamma_2^2}, \tag{A2b}$$

$$\Xi_3 = \frac{2\cos(\phi - \phi')}{q_z^2 + \tilde{\kappa}^2}, \tag{A2c}$$

$$\Xi_4 = 4\frac{\left[\gamma_3\left(q_z^2 + \tilde{\kappa}^2\right) + \gamma_2\gamma_4\right](\cos\phi + \cos\phi') - \left[\gamma_4\left(q_z^2 + \tilde{\kappa}^2\right) - \gamma_2\gamma_3\right](\sin\phi + \sin\phi')}{\gamma_3^2 + \gamma_4^2}. \tag{A2d}$$

For localized phonon modes, $|M(q_{||}, q_z)|^2 |I(k_{||}', k_{||}, \kappa', \kappa, q_z)|^2$ in Eq. (2) can be rewritten in two parts:

$$\frac{|M(q_{||}, q_z)|^2}{Q^2} \left\{ q_{||}^2 |\text{Im}[I(k_{||}', k_{||}, \kappa', \kappa, q_z)]|^2 + q_z^2 |\text{Re}[I(k_{||}', k_{||}, \kappa', \kappa, q_z)]|^2 \right\}, \tag{A3}$$

where

$$|\text{Im}[I(k_{||}', k_{||}, \kappa', \kappa, q_z)]|^2 = |B|^2 |B'|^2 \Xi_{||}/16, \tag{A4a}$$

$$|\text{Re}[I(k_{||}', k_{||}, \kappa', \kappa, q_z)]|^2 = |B|^2 |B'|^2 \Xi_z/16. \tag{A4b}$$

$\Xi_{||} = q_z^2 (\Xi_{||,1} + \Xi_{||,2} + \Xi_{||,3} + +\Xi_{||,4})$ can be expressed in terms of

$$\Xi_{||,1} = \frac{2\cos(\phi + \phi')\left(\gamma_1^2 - 4\gamma_2^2\right) - 8\gamma_1\gamma_2 \sin(\phi + \phi')}{\left(\gamma_1^2 + 4\gamma_2^2\right)^2}, \tag{A5a}$$

$$\Xi_{||,2} = \frac{2[\cos(\phi - \phi') + 1]}{\left(q_z^2 + \tilde{\kappa}^2\right)^2}, \tag{A5b}$$

$$\Xi_{||,3} = \frac{2}{\left(\gamma_1^2 + 4\gamma_2^2\right)}, \tag{A5c}$$

$$\Xi_{||,4} = \frac{8\cos\left(\frac{\phi - \phi'}{2}\right)\left[\gamma_1 \cos\left(\frac{\phi + \phi'}{2}\right) - 2\gamma_2 \sin\left(\frac{\phi + \phi'}{2}\right)\right]}{\left(\gamma_1^2 + 4\gamma_2^2\right)\left(q_z^2 + \tilde{\kappa}^2\right)}, \tag{A5d}$$

and $\Xi_z = \Xi_{z,1} + \Xi_{z,2} + \Xi_{z,3} + \Xi_{z,4}$ can be expressed in terms of

$$\Xi_{z,1} = \frac{2\cos(\phi + \phi')\left[\left(\gamma_1^2 - 4\gamma_2^2\right)(\tilde{\kappa}^2 - g^2) + 8\gamma_1\gamma_2^2\right]}{\left(\gamma_1^2 + 4\gamma_2^2\right)^2} + \frac{\sin(\phi + \phi')4\gamma_2\left[\gamma_1^2 - 4\gamma_2^2 - 4\gamma_1\gamma_2(\tilde{\kappa}^2 - g^2)\right]}{\left(\gamma_1^2 + 4\gamma_2^2\right)^2}, \tag{A6a}$$

$$\Xi_{z,2} = \frac{2\tilde{\kappa}^2[\cos(\phi - \phi') + 1]}{\left(q_z^2 + \tilde{\kappa}^2\right)^2}, \tag{A6b}$$

$$\Xi_{z,3} = \frac{2(g^2 + \tilde{\kappa}^2)}{\left(\gamma_1^2 + 4\gamma_2^2\right)}, \tag{A6c}$$

$$\Xi_{z,4} = \frac{8\cos\left(\frac{\phi - \phi'}{2}\right)\tilde{\kappa}\left[(2\gamma_2 g + \gamma_1\tilde{\kappa})\cos\left(\frac{\phi + \phi'}{2}\right) + (\gamma_1 g - 2\gamma_2\tilde{\kappa})\sin\left(\frac{\phi + \phi'}{2}\right)\right]}{\left(\gamma_1^2 + 4\gamma_2^2\right)\left(q_z^2 + \tilde{\kappa}^2\right)}. \tag{A6d}$$

[1] P. L. Kapitza, J. Phys. USSR **4**, 181 (1941).

[2] T. Nakayama, in *Progress in Low Temperature Physics*, edited by D. F. Brewer (North-Holland, Amsterdam, 1989), Vol. XII, p. 115.

[3] W. A. Little, Can. J. Phys. **37**, 334 (1959); D. A. Neeper and J. R. Dillinger, Phys. Rev. **135**, A1028 (1964); E. T. Swartz, Ph.D. thesis, Cornell University, 1987.

[4] G. L. Pollack, Rev. Mod. Phys. **41**, 48 (1969).

[5] E. T. Swartz and R. O. Pohl, Rev. Mod. Phys. **61**, 605 (1989).

[6] D. G. Cahill, W. K. Ford, K. E. Goodson, G. D. Mahan, A. Majumdar, H. J. Maris, R. Merlin, and S. R. Phillpot, J. Appl. Phys. **93**, 793 (2003).

[7] D. G. Cahill *et al.*, Appl. Phys. Rev. **1**, 011305 (2014).

[8] I. M. Khalatnikov, Zh. Eksp. Teor. Fiz. **22**, 687 (1952); I. M. Khalatnikov and I. N. Adamenko, *ibid.* **63**, 745 (1972) [Sov. Phys. JETP **36**, 391 (1973)].

[9] R. J. Stoner, H. J. Maris, T. R. Anthony, and W. F. Banholzer, Phys. Rev. Lett. **68**, 1563 (1992); R. J. Stoner and H. J. Maris, Phys. Rev. B **48**, 16373 (1993).

[10] A. Debernardi, S. Baroni, and E. Molinari, Phys. Rev. Lett. **75**, 1819 (1995).

[11] G. T. Hohensee, R. B. Wilson, and D. G. Cahill, Nat. Commun. **6**, 6578 (2015).

[12] W. A. Little, Phys. Rev. **123**, 435 (1961).

[13] A. F. Andreev, Zh. Eskp. Teor. Fiz. **43**, 1535 (1962) [Sov. Phys. JETP **16**, 1084 (1963)].

[14] F. Wagner, F. J. Kollarits, and M. Yaqub, Phys. Rev. Lett. **32**, 1117 (1974).

[15] M. I. Kaganov, I. M. Lifshitz, and L. V. Tanatarov, Sov. Phys. JETP **4**, 173 (1957).

[16] P. B. Allen, Phys. Rev. Lett. **59**, 1460 (1987).

[17] M. L. Huberman and A. W. Overhauser, Phys. Rev. B **50**, 2865 (1994).

[18] A. V. Sergeev, Phys. Rev. B **58**, R10199(R) (1998).

[19] G. D. Mahan, Phys. Rev. B **79**, 075408 (2009).

[20] A. Giri, B. M. Foley, and P. E. Hopkins, J. Heat Transfer **136**, 092401 (2014).

[21] H. K. Lyeo and D. G. Cahill, Phys. Rev. B **73**, 144301 (2006).

[22] S. G. Louie and M. L. Cohen, Phys. Rev. Lett. **35**, 866 (1975); Phys. Rev. B **13**, 2461 (1976).

[23] J. Bardeen, Phys. Rev. **71**, 717 (1947); V. Heine, *ibid.* **138**, A1689 (1965).

[24] F. García and F. Flores, *Introduction to the Theory of Solid Surfaces* (Cambridge University Press, Cambridge, UK, 1979).

[25] M. Li, Y. Wang, J. Zhou, J. Ren, and B. Li, Euro. Phys. J. B **88**, 149 (2015).

[26] J. Lombard, F. Detcheverry, and S. Merabia, J. Phys.: Condens. Matter **27**, 015007 (2015).

[27] S. M. Sze and Kwok K. Ng, *Physics of Semiconductor Devices*, 3rd ed. (Wiley Interscience, New York, 2006).

[28] M. A. Stroscio and M. Dutta, *Phonons in Nanostructures* (Cambridge University Press, Cambridge, UK, 2001).

[29] A. Majumdar and P. Reddy, Appl. Phys. Lett. **84**, 4768 (2004).

[30] C. D. Clark, P. J. Dean, and P. V. Harns, Proc. R. Soc. London, Ser. A **277**, 312 (1964).

[31] L. Reggiani, in *Hot Electron Transport in Semiconductors*, edited by L. Reggiani (Springer, Berlin, 1985), p. 66.

[32] C. Jacoboni and L. Reggiani, Rev. Mod. Phys. **55**, 645 (1983).

[33] N. W. Ashcroft and N. D. Mermin, *Solid State Physics* (Harcourt College Publishers, Orlando, 1976), p. 38.

[34] This value is calculated by the Fermi energy of Pt, which is 9.74 eV, from E. Gharibshahi and E. SaionInt. J. Mol. Sci. **13**, 14723 (2012).

[35] W. Mönch, Europhys. Lett. **27**, 479 (1994).

[36] L. Reggiani, S. Bosi, C. Canali, F. Nava, and S. F. Kozlov, Solid State Commun. **30**, 333 (1979).

[37] J. M. Calleja, J. Kuhl, and M. Cardona, Phys. Rev. B **17**, 876 (1978).

[38] C. Monachon and L. Weber, J. Appl. Phys. **113**, 183504 (2013).